Structure and optical properties of α - and γ - cerium sesquisulfide

René Windiks¹ and Erich Wimmer

Materials Design s.a.r.l.
44, avenue F.-A. Bartholdi
72000 Le Mans, France

Leonid Pourovskii

Ecole Polytechnique, Centre de Physique Théorique

91128 Palaiseau Cedex, France

and

Materials Design s.a.r.l.

44, avenue F.-A. Bartholdi

72000 Le Mans, France

Silke Biermann and Antoine Georges

Ecole Polytechnique, Centre de Physique Théorique
91128 Palaiseau Cedex, France

Abstract

Structural and electronic properties of the α - and γ -phases of cerium sesquisulfide, Ce₂S₃, are examined by first-principles calculations using the GGA+U extension of density functional theory. The strongly correlated f-electrons of Ce are described by a Hubbard-type

on-site Coulomb repulsion parameter. A single parameter of U' = 4 eV yields excellent

results for crystal structures, band gaps, and thermodynamic stability for both Ce2S3 al-

lotropes. This approach gives insights in the difference in color of brownish-black α-Ce₂S₃

and dark red γ -Ce₂S₃. The calculations predict that both Ce₂S₃ modifications are insulators

with optical gaps of 0.8 eV (α -phase) and 1.8 eV (γ -phase). The optical gaps are deter-

mined by direct electronic excitations at $\mathbf{k} = \Gamma$ from localized and occupied Ce 4f-orbitals

into empty Ce 5d-states. The f-states are situated between the valence and conduction

bands. The difference of 1 eV between the optical gaps of the two Ce₂S₃ modifications

is explained by different coordinations of the cerium cations by sulfur anions. For both

 Ce_2S_3 modifications the calculations yield an effective local magnetic moment of 2.6 μ_B

per cerium cation, which is in agreement with measurements. The electronic energy of the

 α -phase is computed to be 6 kJ mol⁻¹ lower than that of the γ -phase, which is consistent

with the thermodynamic stability of the two allotropes.

Key words: rare earth alloys and compounds, crystal structure, electronic band structure,

computer simulations

PACS: 71.15.Mb, 61.66.-f, 71.20.-b, 71.27.+a

To whom the correspondence should be addressed. Current address:

Dorfstrasse 63B, 5417 Untersiggenthal, Switzerland

Phone: +41 56 282 04 64, Email: rwindiks@materialsdesign.com

2

1 Introduction

Rare earth (RE) elements are essential ingredients in a large variety of materials of vital technological, economic, and ecological importance. This includes energy-efficient lighting systems, plasma displays, medical imaging, automotive catalysts, permanent magnets, and pigments [1]. These applications depend on the unique structural, electronic, optical, magnetic, and chemical properties of RE compounds. The origin for many of these properties is the presence of localized 4f-electrons interacting with the valence electrons. In this context, the present work focuses on cerium sesquisulfide (Ce_2S_3), which is used as an environmentally responsible pigment with high temperature stability [2]. Beyond this specific application, Ce_2S_3 can be seen as a representative of a large class of RE compounds containing 4f-electrons. Therefore, the approach and results of the present work has implications for many RE-containing compounds and their applications.

The localization of the 4f-electrons involves strong correlation effects which are not captured by current standard methods within density functional theory (DFT). The result is that these DFT calculations fail to reproduce, e.g. the non-metallic ground state of Ce_2S_3 [3, 4] and overestimate the mass density of crystal structures of other cerium compounds [5, 6, 7]. Hence, approaches beyond conventional DFT methods are required to describe Ce_2S_3 realistically from first principles. The present work demonstrates the usefulness of a DFT method extended by a Hubbard-type on-site Coulomb repulsion parameter for treating the Ce_3S_4 realistically from first principles.

Cerium sesquisulfide exists in three allotropic forms [8, 9]. The α -phase is the

low-temperature modification and has a brownish-black (rusty) hue [10]. Above $\sim 900^{\circ}\text{C}$ $\alpha\text{-Ce}_2\text{S}_3$ transforms irreversibly into the dark red (maroon) colored $\beta\text{-phase}$. The $\beta\text{-modification}$ has been described as an oxysulfide with the formula $\text{Ce}_{10}\text{S}_{15-x}\text{O}_x$ [11]. The oxygen can be partially replaced by sulfur. However, a complete substitution appears to be impossible [11], despite other assertions of Picon *et al.* [10]. The structure of the β -phase has been described as complex, but has not been resolved. For these reasons, the β -phase is not considered in the present computational work. The high-temperature allotrope, $\gamma\text{-Ce}_2\text{S}_3$, is preferentially formed between 1100°C and 1200°C. However, $\gamma\text{-Ce}_2\text{S}_3$ can be stabilized at temperatures below 800°C [12, 2]. The melting point of the γ -phase is at $\sim 2100^{\circ}\text{C}$ [10, 13].

The γ -phase of Ce_2S_3 is a nontoxic inorganic high performance pigment of dark red (burgundy) hue, which is used on an industrial scale in the coloration of plastics, paints, and coatings [2]. Optical studies [14, 15] suggest that the dark red color of γ - Ce_2S_3 arise from dipole-allowed excitations of electrons from 4f-states into the empty 5d-states $(4f^15d^0 \rightarrow 4f^05d^1)$ of the same cerium cation. The three modifications of Ce_2S_3 have an insulating nature, as is already clear from their color.

The magnetic susceptibility of α –Ce₂S₃ and γ -Ce₂S₃ at room temperature are similar [10]: 2.9×10^7 (α -phase) and 2.7×10^7 (γ -phase), in SI units. The γ -phase exhibits ferromagnetism below 3 K and the measured effective magnetic moment of each cerium cation is $\mu_{eff} = 2.5 \,\mu_B$ [16, 17, 18]. The magnetic moment is equivalent to that of an isolated Ce³⁺ ion which has the electron configuration [Xe]4 f^1 and the ground state ${}^2F_{5/2}$ [19]. Thorough literature searches did not yield anything about a magnetic ordering of α - Ce₂S₃ at low temperatures. The α - and γ - phases of Gd₂S₃ have the same magnetic ordering at low temperatures [20].

Moreover, α -Gd₂S₃ and γ - Gd₂S₃ are isomorphic to α - Ce₂S₃ and γ -Ce₂S₃, respectively. For these reasons, we shall assume in the following that both α -Ce₂S₃ and γ -Ce₂S₃ are ferromagnetic at low temperatures.

The conduction band (cb) of γ -Ce₂S₃ is mainly formed by empty Ce 5*d*-states while the valence band (vb) consists predominantly of sulfur 3*p*-orbitals [3, 4, 14, 15, 21]. Due to their rather extended character and large energy dispersion Ce 6*s*-states contribute to both the vb and the cb. The measured gap between the upper edge of the vb and the lower edge of the cb of γ -Ce₂S₃, E_g , is between 2.7 eV [15, 22, 23] and 3.3 eV [15]. In agreement with group-theoretical arguments [24] the smaller band gap has been assigned to phonon-assisted (indirect) electronic excitations. The larger band gap is associated with direct electronic transitions. The temperature dependence of E_g between 250 and 350 K is approximately $-0.1~\mu eV~K^{-1}$, which has been derived from γ -La₂S₃ and γ -Dy₂S₃ [24]. Both compounds have the same structural topology as γ -Ce₂S₃. The corresponding values of typical semiconductors like CdS and CdSe are around $-4~\mu eV~K^{-1}$.

Photoconductivity spectra [25] as well as measurements of the photoluminescence [26] of γ -Ce₂S₃ indicate that the occupied 4f-states of cerium cations are energetically located between the vb and the cb. The gap between the 4f-states and the cb obtained from these measurements is in agreement with the optical gap of 1.8–2.0 eV derived from the dielectric function [14, 15]. Up to now, photoemission spectroscopy studies of γ -Ce₂S₃ have not been able to resolve precisely the energetic position of the occupied Ce 4f-states with respect to the vb [27, 15]. However, the measurements of Mauricot *et al.* [25] reveal that the occupied Ce 4f-states are energetically 0.8 eV above the vb.

Earlier band structure calculations within DFT in the local density approximation (DFT-LDA) on model structures for γ -Ce₂S₃ demonstrated qualitatively the importance of 4f-electrons for the optical properties [3, 4]. However, these calculations have several limitations, which hamper quantitative predictions. These limitations mostly stem from the well known inability of DFT-LDA methods to describe correctly the localized 4 f-states. First, when the 4 f-states are treated in the valence, DFT-LDA calculations predict a metallic (Kohn-Sham) band structure for Ce_2S_3 , with f-states at the Fermi level, in contradiction with the insulating nature of this material. The fact that, within DFT-LDA, these f-bands are found to be split off from the sulfur p-bands is indeed suggestive that the optical transitions from 4f to 5d bands are playing an important role in the optical properties. But it is clearly not possible to go beyond this qualitative observation in a pure DFT-LDA framework, let alone to reach a quantitative description of the optical gaps of Ce_2S_3 derivatives [3, 4]. Second, the models used to describe γ - Ce_2S_3 in Refs. [3, 4] did not capture the electrostatics of the real compound adequately. The charges of the cations in the model significantly deviate from that of trivalent cerium. The deviation was one of the factors for the DFT-LDA calculations to underestimate the energy difference between the 4f-states and the vb. The result was an overestimation of the overlap between the 4f-states and the vb and an artificially large splitting of band states on top of the vb [3]. Third, the previous LDA-DFT calculations did not perform structural relaxation studies or attempt to predict crystal structures. However, the electronic structure and, hence, optical properties are very sensitive to interatomic distances. Furthermore, it is widely documented that DFT-LDA and even the generalized gradient approximation (GGA), an extensions of DFT-LDA, severely overestimate the mass density of f-electron compounds when the f-states are treated in the valence [5, 28, 29]. Our own experience with alkali-doped cerium sesquisulfides is that GGA calculations

underestimate the unit cell volume of these compounds by as much as 6% [30].

The main goal of the present study is to gain a deeper understanding of the relations between the chemical composition, the crystal structure, and the optical properties of both α -Ce₂S₃ and γ -Ce₂S₃. Our study addresses both the crystal structure as well as the electronic properties quantitatively within a single computational framework, namely the GGA+U approach. Analogue to the LDA+U method [31], the GGA+U approach uses the DFT framework but extends the GGA description of exchange-correlation effects in the localized 4f-shell by a many-body interaction term. This term is then treated in a mean-field like manner, allowing for a simple description of strong correlation effects within the Ce 4f-states. The GGA+U approach allows for a full optimization of the crystallographic parameters of Ce_2S_3 , and captures the role of the 4f-electrons in the optical transitions. As we shall see, Ce_2S_3 is found to be an f-electron Mott insulator, in which the Ce 4f-states are split into lower occupied and upper unoccupied sub-bands by the strong on-site Coulomb repulsion. Optical transitions responsible for the color of these compounds are between the lower unoccupied Ce 4f-states and the bottom of the Ce 5d-like cb.

2 Crystal structures

The α -phase of Ce₂S₃ crystallizes in an orthorhombic lattice (crystallographic space group *Pnma*). The unit cell contains four formula units with two and three symmetry inequivalent cerium and sulfur ions, respectively [11]. Figure 1(a) illustrates two different kinds of interlocked Ce–S skeletons which are the

coordination polyhedra of the four Ce1 and the four Ce2 cations. The coordination polyhedra (Ce1)S₈ and (Ce2)S₇ have the shapes of a bi-capped trigonal prism and a rather distorted mono-capped octahedron, respectively. The corners of the trigonal prism are S2, S3, and S3' whereas the vertices of the two caps are the sulfur ions S1'. The cap tip of the octahedron is the sulfur ion S2'. Two of the three symmetry inequivalent sulfur anions (S2 and S3) are bound to five cerium cations. The cations form a rectangular pyramid. The five cerium cations encompassing the remaining symmetry inequivalent sulfur anion (S1) form an axial distorted trigonal bipyramid. The Ce–S distances of the two coordination polyhedra are in the range of 2.85–3.14 Å with average distances of 3.01 Å [(Ce1)S₈] and 2.93 Å [(Ce2)S₇].

The crystal structure of γ -Ce₂S₃ has a body-centered cubic lattice. It is isomorphic to the Th₃P₄ structure and contains vacancies on the cationic sublattice [11, 32, 33]. The cerium cations are located on the 12a positions which have the point group symmetry S_4 ; the sulfur anions occupy sites with C_3 symmetry (16c positions). Each cerium cation is coordinated by eight sulfur anions forming a triangular dodecahedron as depicted in Fig. 1(b), with two different nearest-neighbor distances [34]: r(Ce–S)=2.89 Å and r(Ce–S')=3.09 Å. Each sulfur anion is located on a threefold axis and surrounded by six nearest cerium cations, provided all 12a positions are occupied. The six cations form a distorted octahedron. However, when all the 16c and 12a position are occupied with cations and anions, respectively, the stoichiometry would be Ce₃S₄. In order to achieve the stoichiometry of γ -Ce₂S₃ one out of nine cations has to be removed and vacancies on the cerium sublattice, V_{Ce}, have to be created [33]:

$$3\times [Ce_{3}S_{4}] \equiv Ce_{9}S_{12} \stackrel{-Ce}{\longrightarrow} Ce_{8}V_{Ce}S_{12} \equiv 4\times [Ce_{2}S_{3}]$$

Note that both, γ -Ce₂S₃ and Ce₃S₄ have very similar lattice parameters differing only by 0.06% [32, 34]. The tiny volume difference is evidence for a rather rigid Ce-S framework.

Raman spectra of several RE sesquisulfides in the γ -phase give evidence for randomly distributed vacancies [35]. However, simple electrostatic energy calculations predicted that a completely random distribution of the voids on the cerium sublattice yields an energetically less stable ground state than a vacancy ordering such that the resulting crystal structure of γ -Ce₂S₃ has the symmetry of the space group $I\bar{4}2d$ [33]. A highly symmetric ordering of the vacancies is likely in well-annealed γ -phases whereas rapidly quenched samples might have a random distribution of vacancies [33]. Vacancies in the sulfur sublattice are rather unlikely [36].

Figure 1(c) depicts the smallest conventional crystallographic supercell that accommodates the stoichiometry of γ -Ce₂S₃. The supercell is three times as big as the conventional unit cell of Ce₃S₄ and has the composition $4\times[\text{Ce}_8\text{V}_{\text{Ce}}\text{S}_{12}]$. The distances of a cerium cation to its first, second and third nearest cations in γ -Ce₂S₃ are 7.5, 4.8 and 4.0 Å [34]. In this structure the voids on the cation sublattice create three symmetry inequivalent cerium cations. The supercell can be transformed into a primitive unit cell half as large as the conventional cell shown in Fig. 1(c).

3 Computational Method

All GGA+U calculations have been performed with the *Vienna ab initio* simulation package (VASP) [37, 38, 39, 40, 41] as integrated in the MedeA environment [42]. VASP uses the projector-augmented wave (PAW) method [43]

in the implementation of Kresse and Joubert [39]. Exchange- and correlation effects are described within the GGA by the density functional of Perdew, Burke and Ernzerhof [44]. The PAW potentials take into account 12 valence electrons of each Ce $(5s^25p^66s^25d^14f^1)$ and six valence electrons of each S $(3s^23p^4)$ atom. The plane wave energy cutoff has been set to 333 eV and 299 eV for α -Ce₂S₃ and γ -Ce₂S₃, respectively.

Within the present GGA+U approach [40, 45] the strong electron correlation among the 4f-states is described with the parameter U' = U - J. In the latter term, U is the spherically averaged screened Coulomb repulsion energy required for adding an extra electron into the Ce 4f-states and J represents the corresponding screened exchange energy. The GGA+U one-electron potential is defined as $V_{ij}^{\sigma} = \partial E_{GGA}/\partial \rho_{ij}^{\sigma} + U'(0.5\delta_{ij} - \rho_{ij}^{\sigma})$, whereby E_{GGA} is the GGA electronic enenergy, ρ_{ij}^{σ} is the density matrix of f-electrons with spin σ , and δ_{ij} is the delta function. The double counting correction applied is equivalent to that of the fully-localized limit. The case U' = 0 is the limit of pure GGA.

The parameter U' can be calculated from first principles without knowledge of experimental data [46]. In this work however, instead of performing such calculations (which are computationally heavy because of the large numbers of atoms in the unit cell), we have investigated whether U' can be chosen in such a way to reproduce with reasonable accuracy *both* the experimentally measured unit cell volume, as well as the optical gap of the γ -Ce₂S₃ allotrope. We found that the value U' = 4 eV achieves this goal. This value is in agreement with Coulomb repulsion parameters calculated for other cerium compounds [47, 48].

The Kohn-Sham equations are solved self-consistently in their spin-polarized form employing an iterative matrix diagonalization (blocked Davidson scheme) and the spin interpolation of Vosko et al. [49]. The convergence criterion to obtain the energy is 10^{-5} eV. The integration over the first Brillouin-zone is performed using symmetry adapted Monkhorst-Pack grids [50] of **k**-point sets of various size. To calculate energies, energy gradients (atomic forces as well as the stress tensors), and charge densities the **k**-point sets are $3 \times 7 \times 3$ (α -Ce₂S₃) and $3 \times 3 \times 3$ (γ -Ce₂S₃). All **k**-point sets as well as the plane wave energy cutoff has been determined within a convergence test to yield to a numerical precision of 5×10^{-3} eV.

The crystal structures of α -Ce₂S₃ and γ -Ce₂S₃ as described in Sec. 2 have been optimized such that atomic positions and the crystallographic cell parameters are relaxed simultaneously. The optimization procedure has two steps. In the first step, the conjugate-gradient algorithm is used and the optimization stops when all energy gradients are smaller than 0.02 eV Å⁻¹. Then the crystal structures are further refined within a quasi-Newton algorithm with a very tight convergence criterion of 0.002 eV Å⁻¹.

Energy gradients have been calculated with a Gaussian integration method and a smearing of $\sigma=10^{-3}$ eV. The linear tetrahedron method with Blöchl corrections has been used to obtain accurate energies and the self-consistent charge densities. (This integration scheme is inappropriate for calculating energy gradients.) The self-consistent charge densities are used to calculate the band structures and the densities of states (DOS's). All DOS's have been calculated using the linear tetrahedron method without corrections and the same **k**-point sets applied to calculate the energies (see above).

Since the calculations correspond to zero temperature, the two Ce_2S_3 phases adopt the ferromagnetic state. In all calculations the ferromagnetic state is described

with all f-electron spins alligned parallel (spin-up). The band structures and DOS's have been created from the charge density of the electrons with spin-up. This is sufficient since in the present approach only the spin-up states contain occupied f states while the S 3p-vb and Ce 5d/6s-conduction states are similar for both spin orientations.

4 Results and discussion

4.1 α-Phase

Table 1 summarizes calculated lattice parameters and interionic distances of the two interlocked (Ce1)S₈ and (Ce2)S₇ skeletons shown in Fig. 1(a). As announced above, the chosen value U' = 4 eV yields a relative error on the unit cell volume which is smaller than 1% in comparison to experiments. A comparison with the corresponding experimental distances reveals remarkable agreement. Most of the calculated distances are less than 0.9% larger than those determined from x-ray diffraction measurements. Exceptions are the calculated cell length c and the bond lengths r(Ce1-S1') and r(Ce2-S3) which are nearly equal or smaller, respectively, than the corresponding measured distances. The discrepancies are almost zero for c, -0.1% (r(Ce2–S3), and around -1.2% for the longest of the two Ce1–S1' distances. The calculations tend to strengthen one of the Ce1–S1' bonds at the expense of the other thereby slightly decreasing the sulfur coordination of Ce1. Note that the measurements and the calculations yield for the two distances r(Ce1-S1') average values of 3.12 and 3.11 Å, respectively. The average of the calculated distances between cerium and sulfur within the (Ce1)S₈ and (Ce2)S₇ skeletons are 3.02 and 2.94 Å, respectively. Both distances are only between 0.4

and 0.7% larger than the corresponding distances of the x-ray structure. Apart from r(Ce1-Ce1) all other calculated Ce–Ce distances are larger than the measured values with deviations not larger than 0.5%.

The energy of formation, E_{form} , is a measure for the stability and is the difference between the energy of the entire system and the energies of the electronic ground state of the constitutive elements in their standard state. For α -Ce₂S₃ the calculations yield $E_{form} = -820 \text{ kJ mol}^{-1} \text{ Ce}_2\text{S}_3$.

Figure 2 shows the band structure and the corresponding partial DOS (PDOS) calculated for the fully optimized crystal structure of α -Ce₂S₃. The electronic bands are drawn along the standard pathway within the irreducible wedge of the Brillioun zone of simple orthorhombic lattices. The PDOS illustrates that the vb, i.e. the occupied and evenly dispersed electron bands below approximately -0.8 eV, are mainly formed by S 3p-orbitals with contributions of Ce 3d-orbitals. This indicates a significant covalent contribution to the bonding in α -Ce₂S₃.

On top of the vb, i.e. the occupied electron bands between -0.8 eV and zero energy are two kinds of occupied 4f-orbitals namely those of the cations Ce1 and Ce2, respectively. In the following occupied 4f-states are termed as lower Hubbard bands (LHB's). Both LHB's have rather large admixtures of S 3p-states. This indicates a participation of Ce 4f-orbitals in the covalent bonding. The PDOS of Fig. 2(b) shows that the LHB of the Ce1 cations is located at a lower energy than the LHB of the Ce2 cations. The main reason for the different positions must be the different sulfur environments of the Ce1 and Ce2 cations as depicted in Fig. 1(a). The calculations yield almost one f-electron localized on each cerium cation. The computed occupation numbers of the 4f-states, n_f , of the two symmetry inequivalent cerium cations are 1.12 (Ce1) and 1.14 (Ce2).

Occupation numbers of $n_f > 1$ are consistent with admixtures of S 3p-states to Ce 4f-orbitals. Assuming that the total orbital moment of the electronic ground state of all cerium cations is J = 5/2 the effective local magnetic moment is around 2.6 μ_B per cerium cation. This is consistent with experiment.

The LHB's have different features within the chosen part of the Brillouin zone. On the one hand the LHB's have significant dispersion (on the scale of ~ 0.5 eV) between $\mathbf{k} = T$ and the center of the line between $\mathbf{k} = \Gamma$ and $\mathbf{k} = X$ (Σ line). On the other hand the LHB's are rather flat between the center of the Σ line and $\mathbf{k} = Y$ and along the line between $\mathbf{k} = R$ and $\mathbf{k} = T$. The LHB's are almost degenerate at $\mathbf{k} = R$ and $\mathbf{k} = S$.

The smallest gap between the upper edge of the LHB of Ce2 and the lower edge of the unoccupied states (cb) is 0.8 eV and is at $\mathbf{k} = \Gamma$. At the same \mathbf{k} -point is the smallest separation between the vb and the cb (1.34 eV). The cb has predominantly Ce 5d-character with small contributions of S 3p-orbitals. Like the LHB's but more distinct, the cb exhibits a strong dispersion between k = T and k = X. The PDOS of the cb at its lower edge is tiny and increases in small steps between 0.7 and 1.8 eV.

The inset of Fig. 2(b) depicts the presence of Ce 6s- and Ce 6p-orbitals in the relevant electron bands of Fig. 2(a). Their contributions within the relevant energy range around the Fermi energy are relatively small because the 6s- and 6p-states are spatially extended and energetically dispersed. Inside the cb between 2.0 and 4.2 eV are unoccupied Ce 4f-orbitals which form the upper Hubbard band (UHB).

The band dispersions of the LHB and the cb are examined in terms of an orbital-projected band-structure (sometimes called "fat-band" representation). Figure 3 illustrates contributions of atomic states to relevant energy bands of Fig.

2(a) between $\mathbf{k} = T$ and $\mathbf{k} = X$ at different \mathbf{k} -points. The three lowest unoccupied states at $\mathbf{k} = \Gamma$ are due to anti-bonding interactions between cerium 5d- and sulfur 3p-states. The contribution of S 3p-orbitals to the three states is between 5 and 15% whereby only states of the atoms S2 and S3 are involved. Admixtures of 3p-orbitals of S1 are negligibly small. The corresponding bonding states are located between -1.9 and -2.3 eV. The splitting between bonding and antibonding states of Ce1 and S3 is between 0.7 and 1.4 eV smaller than that of Ce2 and S2. The smaller splitting and, hence, the distinct dispersion of the two lowest unoccupied bands is due to smaller overlap between 5d- and 3p-orbitals of Ce1 and S3, respectively.

The dispersions at the upper edge of the LHB are also due to admixtures of S 3p-orbitals to the Ce 4f-states. The two highest occupied electronic states of the LHB contain at $\mathbf{k} = \Gamma$ both 44% of S 3p-orbitals whereby all sulfur ions contribute equally. The remaining contributions come from the 4f-states of Ce1 and Ce2, respectively (cf. Fig. 3). The contributions of all cerium cations is consistent with the small tails of the 4f-states in the PDOS of Fig. 2(b) at zero energy. In fact the entire vb contains contributions of 4f-states which decrease towards lower energies.

The calculated GGA+U band structure yields insight into the optical properties of α -Ce₂S₃ and its color. The dispersion at the lower edge of the cb at $\mathbf{k} = \Gamma$ causes the rather small direct band gap of 0.8 eV. However, this gap is between states of Ce1 and Ce2. Since the color of the cerium sesquisulfides is determined by the excitations $4f^15d^0 \rightarrow 4f^05d^1$ taking place on the same site we have to distinguish between two optical transitions. The orbital-projected band-structure of Fig. 3 reveals that the smallest 4f-5d gaps of Ce1 and Ce2 are about 1.0 and 1.7 eV, respectively. Consequently, the reason why α -Ce₂S₃ has a brownish-black color is

twofold. The cerium cations Ce2 absorb photons with energies larger than 1.7 eV which would lead to a dark red color. The smaller gap of $\sim 1.0 \text{ eV}$ (Ce1 cations) is responsible that all radiation of the visible range is absorbed. However, the absorption of radiation with an energy between 0.7 and 1.8 eV (near infrared and red light) is relatively low because the density of states is rather small in this region [compare Fig. 2(b)]. This effect leads to the black shade. Dark red mixed with black yields a brown-black hue.

4.2 γ-Phase

Table 2 summarizes lattice parameters and selected interionic distances calculated for γ -Ce₂S₃ and compares the values with that of the x-ray structure of Ref. [34]. Again, the chosen value of U' yields a calculated unit-cell volume which is less than 1% larger than that determined from experiment. The deviation between the calculated and measured average Ce–S bond lengths is negligibly small. The smallest calculated Ce–Ce distance which is 2% smaller than that determined from the x-ray structure. The reason for the cell expansion is a growth of the voids located on the cation sublattice [cf. red spheres of Fig. 1(c)]. The calculated structure has distances between the center of the voids, Q, and the nearest sulfur anions which are between 3.1% and 4.0% larger than those of the experimental structure.

The $I\bar{4}2d$ structure of Fig. 1(c) has three symmetry inequivalent cerium cations and sulfur anions, respectively. Two of the symmetry inequivalent cerium cations have clearly distinguishable bond distances of $r(\text{Ce-S})\sim2.90$ and $r(\text{Ce-S'})\sim3.10$ Å. However, the third kind of cations has an almost continuous spectrum of bond length to its eight nearest sulfur anions in the range of 2.90 and 3.30 Å. Due to the

vacancies two of the three symmetry inequivalent sulfur anions are bound to five cerium cations only. All the penta-coordinated sulfur anions have three Ce–S bonds and two Ce–S' bonds [cf. Fig. 1(b)]. The six-fold coordinated sulfur anions have Ce–S distances, which are between 1 and 2% larger than the calculated average bond lengths of Tab. 2. The calculated energy of formation for the γ -phase is $\Delta E_{form} = -814$ kJ mol⁻¹ Ce₂S₃.

Figure 4 depicts the band structure and PDOS calculated for the fully optimized $Ce_{16}S_{24}$ supercell which is the primitive cell of that shown in Fig. 1(c). Comparison with Fig. 2 reveals similarities between the electronic structures of the α -phase and the γ -modification, but also significant differences which will be addressed in more details in Sec. 5. Up to an energy of -1.0 eV, the vb is mainly formed by S 3p-orbitals with small contributions of Ce 4f-states. Between -1.2 and -0.5 eV the vb has increasing admixtures of Ce 4f-states. The region of the occupied states above -0.5 eV (directly on top of the vb) is dominated by the LHB with significant components of S 3p-states. The difference to the PDOS of the α -phase is that the LHB of γ -Ce₂ S₃ has one maximum only at around -0.4 eV. The width of the LHB is around 0.5 eV without any distinct dispersion. The location of the 4f LHB is in good agreement with available photoelectron spectroscopy data, but inferring its width from these experiments is difficult given the resolution [15].

The single maximum of the LHB in the PDOS is evidence for cerium cations which are electronically and magnetically equivalent. This is consistent with the fact that the calculations yield for each cerium cation occupation numbers of $n_f = 1.14$. Occupation numbers larger than one indicate admixtures of other band states, mainly S 3p-orbitals. As in the case of α -Ce₂S₃ the cerium cations of the γ -phase have a local effective magnetic moment of $2.6~\mu_B$.

The cb has predominantly Ce 5d character with small admixtures of S 3p-states and has its largest dispersion around $\mathbf{k} = \Gamma$. At the same \mathbf{k} -point is the smallest direct gap between the maximum of the LHB and the cb minimum of around 1.8 eV which is in fact in the range of measured optical gaps between 1.8 and 2.0 eV [15, 22, 51, 52]. Thus the present calculations on γ -Ce₂S₃ result in a dark red color. The rather weak dispersion of both the LHB and of the Ce 5d bands at the bottom of the cb [see Fig. 4(a)] implies a rather sharp absorption edge. This is in contrast with the α -allotrope in which both the LHB and the 5d cb are more disperse. The smallest gap between the vb and the cb is 2.3 eV, also at $\mathbf{k} = \Gamma$. The minimum of the lower edge of the UHB is located approximately 2.8 eV above zero energy.

5 Comparison between the Ce_2S_3 modifications

Both allotropes have crystal structures with a relatively high average coordination of eight sulfur atoms around each Ce atom. The mass density of the two Ce_2S_3 phases calculated from the optimized crystal structures is similar: 5.10 Mg m⁻³ (α -phase) and 5.13 Mg m⁻³ (γ -phase). For comparison the experimentally determined mass densities for α -Ce₂S₃ and γ -Ce₂S₃ are 4.95 and 5.18 Mg m⁻³ [10]. The calculations predict that the electronic energy of the α -phase is 6 kJ mol⁻¹ Ce₂S₃ lower (i.e. more stable) than that of the γ -phase. This is in agreement with the fact that α -Ce₂S₃ is the low temperature configuration. In order to be more stable at higher temperatures the γ -phase must have a larger entropy than the α -modification. This is plausible because the γ -phase contains vacancies on the cationic sublattice. The voids might cause more low energy lattice phonons in the γ -phase than in the α -phase. A lowering of phonon frequencies leads to a higher vibrational entropy. Furthermore, the distribution of

voids in the lattice adds a configurational entropy, which also tends to stabilize the γ -phase at elevated temperatures.

Figure 5 compares the partial density of states of α -Ce₂S₃ and γ -Ce₂S₃ in the energy range of -37 to 10 eV. Overall, the electronic structures of the two allotropes have common features. The bonding between Ce and S atoms has significant covalent components. It is dominated by the interaction between Ce 5d- and S 3p-orbitals. The centers of the bonding and anti-bonding p-d bands are approximately 7 eV apart in both compounds (cf. Fig. 5).

In both modifications, the effective one-particle energy of this LHB is at the top of the S 3p vb. This leads to a hybridization between Ce 4f- and S 3p-orbitals. Electronic excitations in the visible part of the spectrum involve transitions from the occupied LHB into the cb, which is dominated by Ce 3d-levels.

However, the present calculations reveal a major distinction between the $\alpha-$ and $\gamma-$ allotropes, due to the structural differences. The presence of two different coordination environments of the cerium cations in the α -phase causes a splitting near the minimum of the cb and also within the occupied 4f-states at the top of the vb (Figs. 2 and 5). As a consequence, the optical transitions at 1.8 eV responsible for the red color are superimposed by transitions, which start around 0.8 eV. Furthermore, this distinction between the two types of Ce cations in the α -phase is noticeable also in the Ce 5s- and Ce 5p-semi-core states at -34 and -17 eV, respectively (Fig. 5). Both states are split by about 0.5 eV whereby the 5s and 5p-states of Ce1 are located at lower energies than that of Ce2. This implies that the effective potential for electrons around Ce1 is more attractive than around Ce2.

6 Summary and conclusions

The present GGA+U calculations yield a very good description of the crystal structures and of the chromatic properties of α -Ce₂S₃ and γ -Ce₂S₃ involving 4f-electrons explicitely. With a Coulomb repulsion parameter of U' =4 eV the calculated cell volume and most of the interionic distances for both Ce₂S₃ phases are less than 1% larger than that determined from x-ray diffraction measurements. This is comparable to the accuracy of standard GGA calculations as applied to systems without f-electrons. This is a major improvement over standard GGA calculations, which underestimate the cell volume of Ce₂S₃ derivatives by as much as 6% and fail to predict their semiconducting character [30].

With the same U' parameter the present calculations yield effective one-electron energies, which allow a quantitative interpretation of optical transitions and thus accounts for the colors of the two Ce_2S_3 allotropes in a satisfactory manner. The vb and cb of both allotropes are dominated by S_3p and Ce_5d -states, respectively. In both phases the occupied Ce_5d -states are energetically located between the vb and cb, whereby the smallest gap between the occupied Ce_5d - and the empty S_5d -states (Δ_{4f-5d}) is direct and located at $\mathbf{k} = \Gamma$.

For the α -phase the calculations yield $\Delta_{4f-5d}=0.8$ eV and a rather small density of states in the range of 0.8–1.5 eV above the vb. The small density of states is due to three low-lying unoccupied bands with strong dispersion and corresponds to low absorption of radiation. The dispersion is related to the (Ce1)S₈ coordination polyhedron and it is the reason for the smaller optical band gap and explains the brownish-black hue α -Ce₂S₃. The dark red color (burgundy) of the γ -Ce₂S₃ is due to Δ_{4f-5d} =1.8 eV and a rather steep increase of the density of states around the

lower edge of the cb. The γ -allotrope is charcaterized by somewhat less dispersive bands and hence a sharper absorption edge.

Thus, the present calculations provide an explanation for the difference of 1 eV in the optical gaps of α -Ce₂S₃ and γ -Ce₂S₃. The main factor is the presence of two types of Ce cations in the α -phase with two different coordination environments and the related difference of 3% between the average Ce–S bond distances in the two allotropes. Despite the different sulfur environments the calculations yield for cerium cations effective local magnetic moments of 2.6 μ_B which is in agreement with magnetic measuremts.

It is gratifying that the computed electronic energy of the low-temperature modification (α -Ce₂S₃) is lower by 6 kJ mol⁻¹ (per formula unit) than that of the high-temperature modification (γ -Ce₂S₃). At low temperatures, the Gibbs free energy, which determines phase stabilities, is therefore lower for the α -phase. At elevated temperatures, the presence of vacancies in the γ -phase is expected to enhance the vibrational and configurational entropy, thus stabilizing the high-temperature phase.

The present GGA+U approach offers a satisfactory description of the Ce 4f-states in terms of structural and optical properties. However, the introduction of the on-site Coulomb repulsion does not cure the drawback of standard DFT methods of underestimating the gap between the itinerant S 3p- and the Ce 5d-band states. The smallest calculated direct gaps between the vb and the cb of γ -Ce₂S₃ is computed to be 2.3 eV. This is approximately 1 eV smaller than the value determined from optical, photoconductivity, and photoluminescence spectra. The same band gap calculated for α -Ce₂S₃ is about 1.3 eV and probably also underestimated by 1 eV. A remedy of this problem might be the combination of

GGA+U and GW techniques [53].

In conclusion, the present work demonstrates that the GGA+U approach is successful in describing quantitatively the structural and electronic properties of α-Ce₂S₃ and γ-Ce₂S₃. The GGA+U approach overcomes a major shortcoming of standard GGA band structure calculations, which incorrectly yields a metallic bandstructure with 4f-states at the Fermi level. Instead, we found Ce_2S_3 to be an f-electron Mott insulator, in which strong correlation effects open up a Mott gap within the 4f-states, between a LHB and an UHB. The LHB is found to play a key role in the physical properties of these compunds, since the optical transitions responsible for their color are between the top of the LHB and the bottom of the 5d cb. Furthermore, subtle differences in the calculated electronic structure of the two allotropes (most notably the presence of two inequivalent cerium sites in the α -modification, as well as more dispersive bands) give insight into the differences in the optical properties and color of these materials. The present GGA+U methodology applied here to RE compounds, could also be used to predict structural and opto-electronic properties of materials where RE elements are used as dopants. This capability will be particularly useful in the design and improvements of materials for lighting and display technologies with major benefits for our society and the environment.

Acknowledgements

This work has been supported by the European Commission within its programme Research and Training Network "Psi-k f-electrons" Contract HPRN-CT-2002-00295, as well as by Ecole Polytechnique and CNRS. The authors are grateful to the other participants of this Network and to Axel Svane for coordination. The authors are

grateful to Paul Saxe, Walter Wolf, Alexander Mavromaras, and Benoit Leblanc (Materials Design) and to Jan Tomczak, Alexander Poteryaev (Ecole Polytechnique) for useful discussions.

References

- [1] G. B. Haxel, J. B. Hedrick, G. J. Orris, Rare Earth Elements Critical Resources for High Technology, Fact-Sheet 087-02, US Geology Survey, 2002.
- [2] H. M. Smith (Ed.), High performance pigments, Wiley-VCH, Weinheim, 2002, p. 27.
- [3] M.-A. Perrin, E. Wimmer, Phys. Rev. B 54 (4) (1996) 2428.
- [4] V. Zhukov, R. Mauricot, P. Gressier, M. Evain, J. Solid State Chem. 128 (2) (1997) 197.
- [5] S. Fabris, S. de Gironcoli, S. Baroni, G. Vicario, G. Balducci, Phys. Rev. B 71 (2005) 041102.
- [6] G. Kresse, P. Blaha, J. L. F. D. Silva, M. V. Ganduglia-Pirovano, Phys. Rev. B 72 (2005) 237101.
- [7] S. Fabris, S. de Gironcoli, S. Baroni, G. Vicario, G. Balducci, Phys. Rev. B 72 (2005) 237102.
- [8] F. Marrot, A. M. J.-C. T. P. Macaudière, P. Maestro, J. Alloys Comp. 259 (1997) 145.
- [9] S. Roméro, A. Mosset, J.-C. Trombe, P. Macaudière, J. Mater. Chem. 7 (8) (1997) 1541.
- [10] M. Picon, L. Domange, J. Flahaut, M. Guittard, M. Patrie, Bull. Soc. Chim. France 2 (1960) 221.
- [11] T. Schleid, P. Lauxmann, Z. Anorg. Allg. Chem. 625 (1999) 1053.
- [12] J. C. Trombe, M. Verelst, J. Alloys and Comp. 323-324 (2001) 66.

- [13] J. R. Henderson, M. Muramoto, E. Loh, J. B. Gruber, J. Chem. Phys. 47 (9) (1967) 3347.
- [14] R. Dagys, G.-J. Babonas, G. Pukinskas, Phys. Rev. B 51 (11) (1995) 6995.
- [15] C. Witz, D. Huguenin, J. Lafait, S. Dupont, M. L. Theye, J. Appl. Phys. 79 (4) (1996) 2038,
- [16] G. Becker, J. Feldhaus, K. Westerholt, S. Methfessel, J. Magn. Magn. Mater. 6 (1977) 14.
- [17] J. C. Ho, S. M. A. Taher, J. B. Gruber, K. A. G. Jr., Phys. Rev. Lett. 26 (3) (1982) 1369.
- [18] I. Mörke, E. Kaldis, P. Wachter, Phys. Rev. B 33 (5) (1986) 3392.
- [19] The magnetic moment is given as $\mu_{eff} = g\sqrt{J(J+1)}\mu_B$, g=1.5+[S(S+1)-L(L+1)]/[2J(J+1)].. N. N. Greenwood, A. Earnshaw, Chemistry of the elements, Pergamon Press, Oxford, 1984.
- [20] S. Ebisu, Y. Iijima, T. Iwasa, S. Nagata, J. Phys. Chem. Solids 65 (2004) 1113.
- [21] G. Babonas, R. Dagys, G. Pukinskas, Phys. Stat. Sol. B 153 (1989) 741.
- [22] A. V. Golubkov, A. V. Prokofiev, A. I. Shelykh, Phys. Solid State 37 (6) (1995) 1028.
- [23] A. V. Prokofiev, A. I. Shelykh, B. T. Melekh, J. Alloys Comp. 242 (1-2) (1996)41.
- [24] V. P. Zhuze, A. A. Kamarzin, M. G. Karin, K. K. Sidorin, A. I. Shelykh, Sov. Phys. Solid State 21 (11) (1979) 1968.
- [25] R. Mauricot, J. Bullot, J. Wery, M. Evian, Mat. Res. Bull. 31 (3) (1996) 263.
- [26] R. Mauricot, J. Dexpert-Ghys, M. Evian, J. Lum. 69 (1996) 41.
- [27] S. Kaciulis, A. Latisenka, A. Plesanovas, Surf. Sci. 251-252 (1991) 330.
- [28] S. Savrasov, G. Kotliar, Phys. Rev. Lett. 84 (16) (2000) 3670.
- [29] N. V. Skorodumova, R. Ahuja, S. I. Simak, I. A. Abrikosov, B. Johansson, B. I. Lundqvist, Phys. Rev. B 64 (2001) 115108.

- [30] R. Windiks, L. Pourovskiy, A. Georges, E. Wimmer, in preparation.
- [31] V. Anisimov, F.Aryasetiawan, A. Lichtenstein, J. Phys: Condens. Matter 9 (1997) 767.
- [32] W. H. Zachariasen, Acta Cryst. 2 (1949) 291.
- [33] F. L. Carter, J. Solid State Chem. 5 (1972) 300.
- [34] R. Mauricot, P. Geissler, M. Evian, R. Bree, J. Alloys Comp. 223 (1) (1995) 130.
- [35] D. S. Knight, W. B. White, Spectrochimica Acta A: Molec. Spectr. 46 (3) (1990) 381.
- [36] B. A. Kolesov, A. A. Kamarzin, V. V. Sokolov, J. Struct. Chem. 38 (4) (1997) 544.
- [37] G. Kresse, J. Furthmüller, Phys. Rev. B 54 (1996) 11169.
- [38] G. Kresse, J. Furthmüller, Comput. Mat. Sci. 6 (1996) 15.
- [39] G. Kresse, D. Joubert, Phys. Rev. B 59 (3) (1999) 1758.
- [40] A. Rohrbach, J. Hafner, G. Kresse, Phys. Rev. B 69 (2004) 0754134.
- [41] J. Paier, R. Hirschl, M. Marsman, G. Kresse, J. Chem. Phys. 122 (2005) 234102.
- [42] Materials Design, Medea 2.0, www.materialsdesign.com (2005).
- [43] P. E. Blöchl, Phys. Rev. B 50 (24) (1994) 17953.
- [44] J. P. Perdew, K. Burke, M. Ernzerhof, Phys. Rev. Lett. 77 (18) (1996) 3865.
- [45] S. L. Dudarev, G. A. Botton, S. Y. Savrasov, C. J. Humphreys, A. P. Sutton, Phys. Rev. B 57 (3) (1998) 1505.
- [46] M. Cococcioni, S. de Gironcoli, Phys. Rev. B 71 (2005) 035105.
- [47] J. F. Herbst, R. E. Watson, J. W. Wilkens, Phys. Rev. B 17 (8) (1978) 3098.
- [48] S. Fabris, G. Vicario, G. Balducci, S. de Gironcoli, S. Baroni, J. Phys. Chem. B 109 (2005) 22860.
- [49] S. Vosko, L. Wilk, M. Nusair, Can. J. Phys. 58 (1980) 1200.

- [50] H. J. Monkhorst, J. D. Pack, Phys. Rev. B 13 (12) (1976) 5188.
- [51] A. V. Prokofiev, A. I. Shelykh, A. V. Golubkov, I. A. Smirnov, J. Alloys Comp. 219 (1995) 172.
- [52] R. Dagys, G.-J. Babonas, J. Solid State Chem. 109 (1994) 30.
- [53] M. Shishkin, G. Kresse, Phys. Rev. B 74 (2006) 035101.

List of Figures

1	(color online) Structural features of cerium sesquisulfide allotropes. Blue and yellow spheres represent cerium cations and sulfur anions, respectively. (a) Coordination polyhedra of the symmetry inequivalent cerium cations Ce1 and Ce2 of α -Ce ₂ S ₃ . (b) Coordination polyhedron of Ce cations in γ -Ce ₂ S ₃ . The sulfur anions S and S' are within and out of the drawing plane, respectively. (c) Smallest conventional unit cell of γ -Ce ₂ S ₃ with a stoichiometric amount of cerium vacancies (red spheres). The composition of the super cell is Ce ₃₂ S ₄₈ and has the highest symmetry possible (space group $I\bar{4}2d$).	28
2	(color online) Electronic structure of $\alpha\text{-Ce}_2S_3$ around the Fermi energy; (a) band structure and (b) partial DOS calculated for the fully optimized crystal structure. Arrows indicate relevant direct band gaps. The energy axes are labeled relative to the energy of the highest occupied band state. The latter is set to zero and is denoted by dashed lines. VB – valence band, CB – conduction band, UHB and LHB – upper and lower Hubbard bands, respectively.	29
3	(color online) Contributions of atomic states per k -point to particular electronic bands of α -Ce ₂ S ₃ between $k=T$ and X as shown in Fig. 2. The thicker the electronic bands the larger the contribution of particular atomic states. Significant contributions of specific atomic states are indicated at $\mathbf{k} = \Gamma$. Asterisks denote anti-bonding interactions. More details are given in the legend of Fig. 2.	30
4	(color online) Electronic structure of pure γ -Ce ₂ S ₃ around the Fermi energy. (a) Band structure and (b) partial density of states calculated for the fully optimized system Ce ₁₆ S ₂₄ (space group $I\bar{4}2d$). More details are given in the legend of Fig. 2.	31
5	(color online) Calculated partial density of states of two Ce_2S_3 modifications in the energy range between -37 and 10 eV.	32

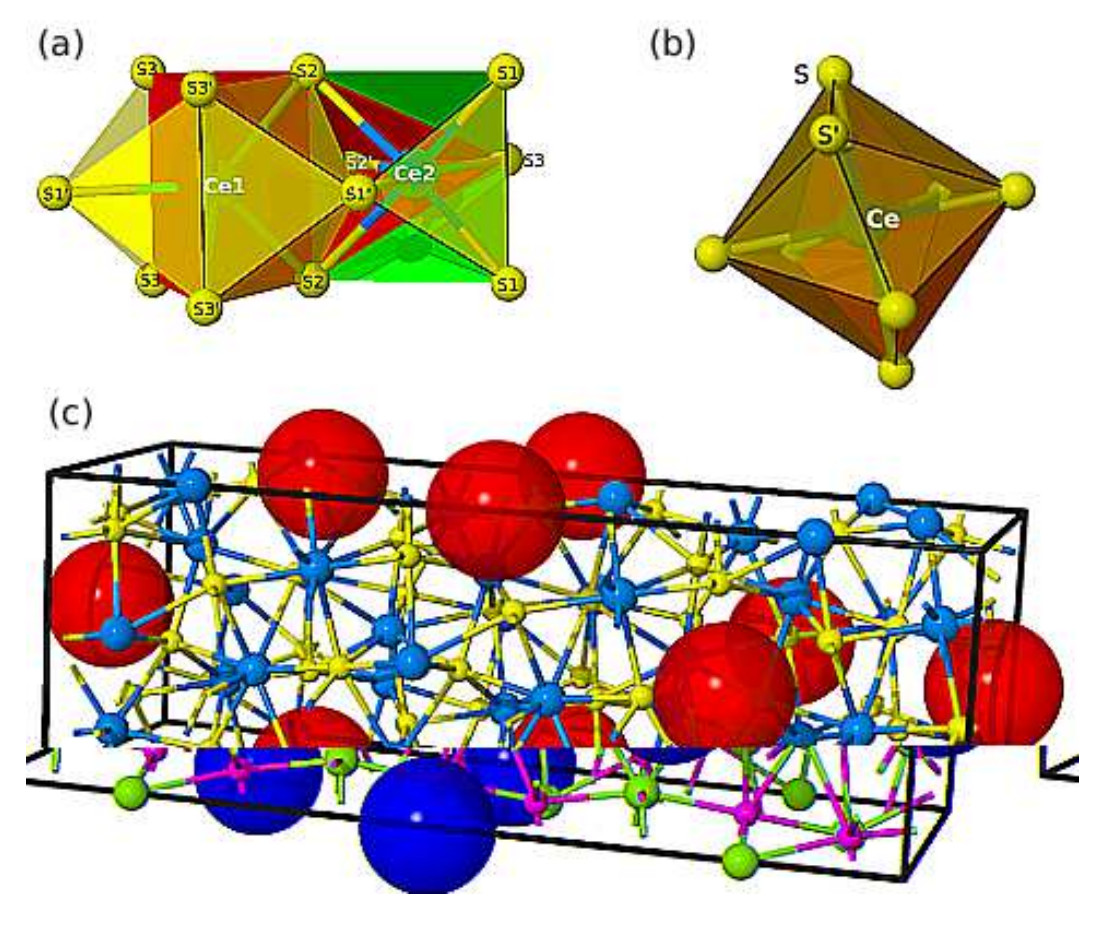


Fig. 1. (color online) Structural features of cerium sesquisulfide allotropes. Blue and yellow spheres represent cerium cations and sulfur anions, respectively. (a) Coordination polyhedra of the symmetry inequivalent cerium cations Ce1 and Ce2 of α -Ce₂S₃. (b) Coordination polyhedron of Ce cations in γ -Ce₂S₃. The sulfur anions S and S' are within and out of the drawing plane, respectively. (c) Smallest conventional unit cell of γ -Ce₂S₃with a stoichiometric amount of cerium vacancies (red spheres). The composition of the super cell is Ce₃₂S₄₈ and has the highest symmetry possible (space group $I\bar{4}2d$).

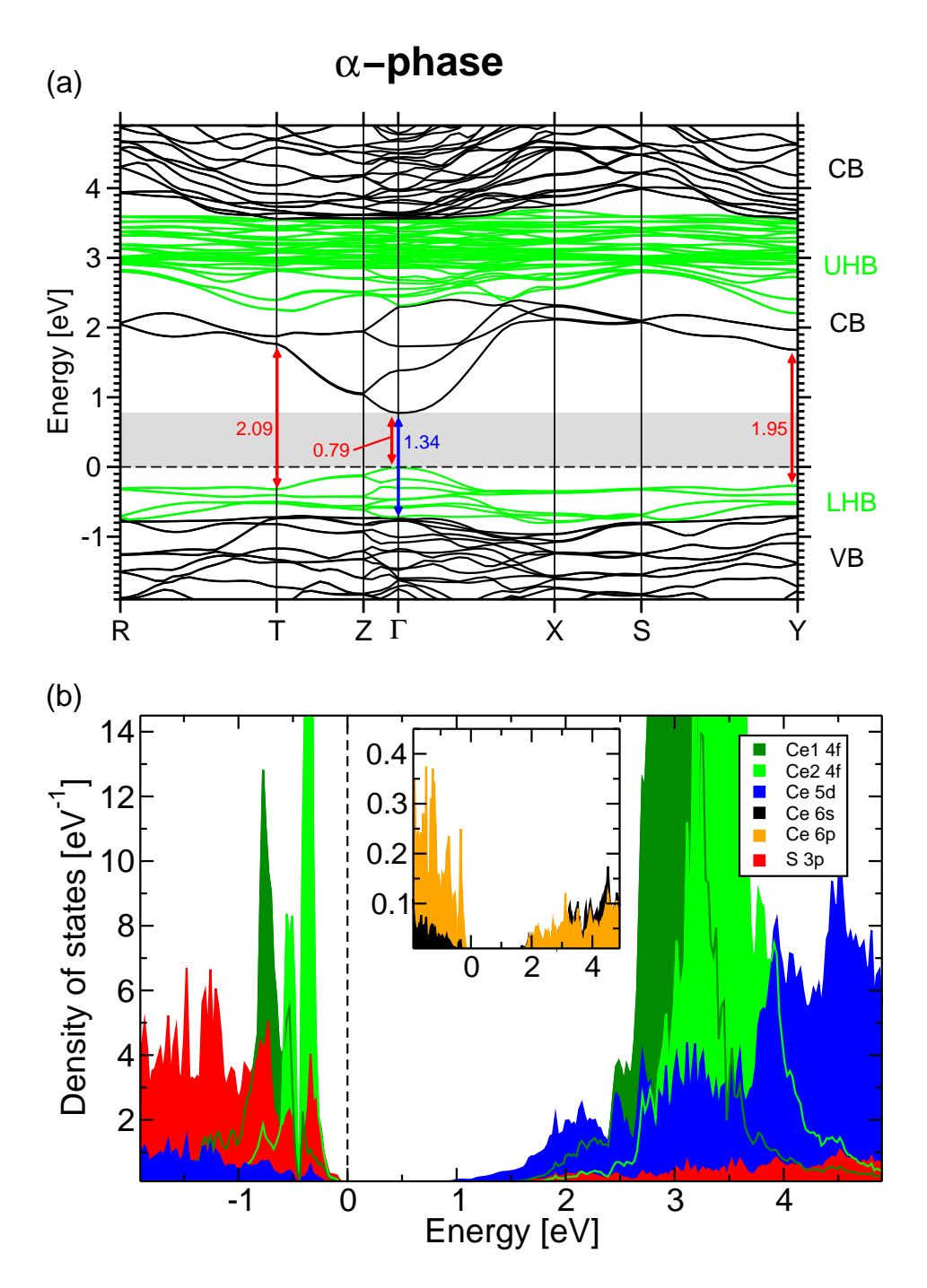


Fig. 2. (color online) Electronic structure of α -Ce₂S₃ around the Fermi energy; (a) band structure and (b) partial DOS calculated for the fully optimized crystal structure. Arrows indicate relevant direct band gaps. The energy axes are labeled relative to the energy of the highest occupied band state. The latter is set to zero and is denoted by dashed lines. VB – valence band, CB – conduction band, UHB and LHB – upper and lower Hubbard bands, respectively.

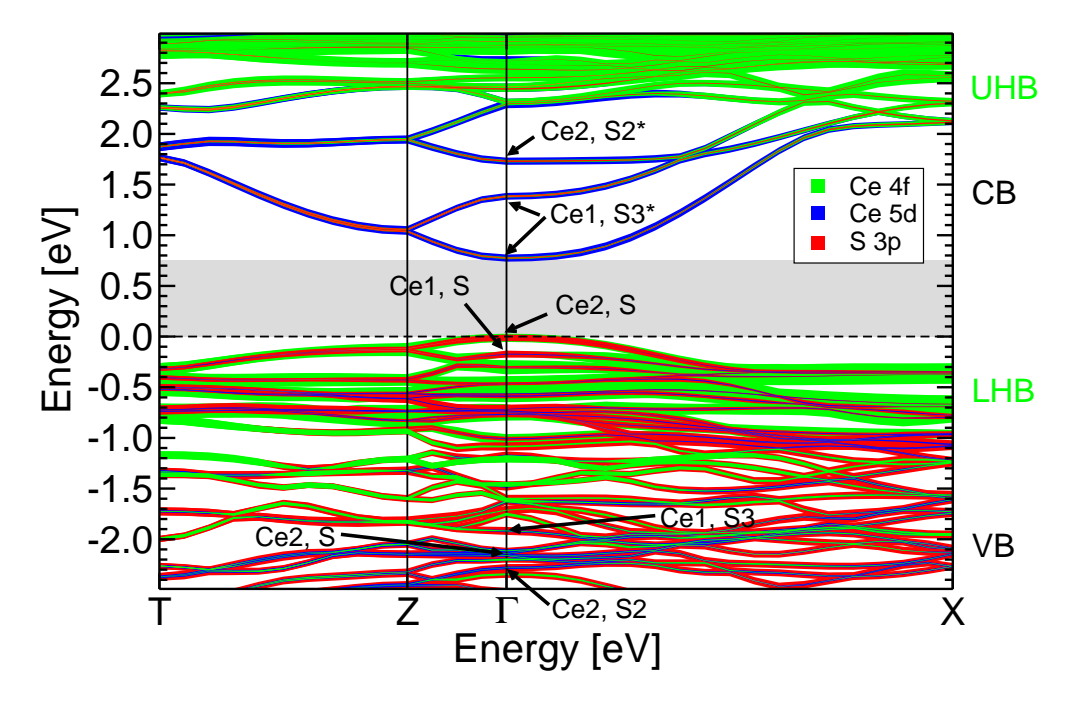


Fig. 3. (color online) Contributions of atomic states per **k**-point to particular electronic bands of α -Ce₂S₃ between k = T and X as shown in Fig. 2. The thicker the electronic bands the larger the contribution of particular atomic states. Significant contributions of specific atomic states are indicated at $\mathbf{k} = \Gamma$. Asterisks denote anti-bonding interactions. More details are given in the legend of Fig. 2.

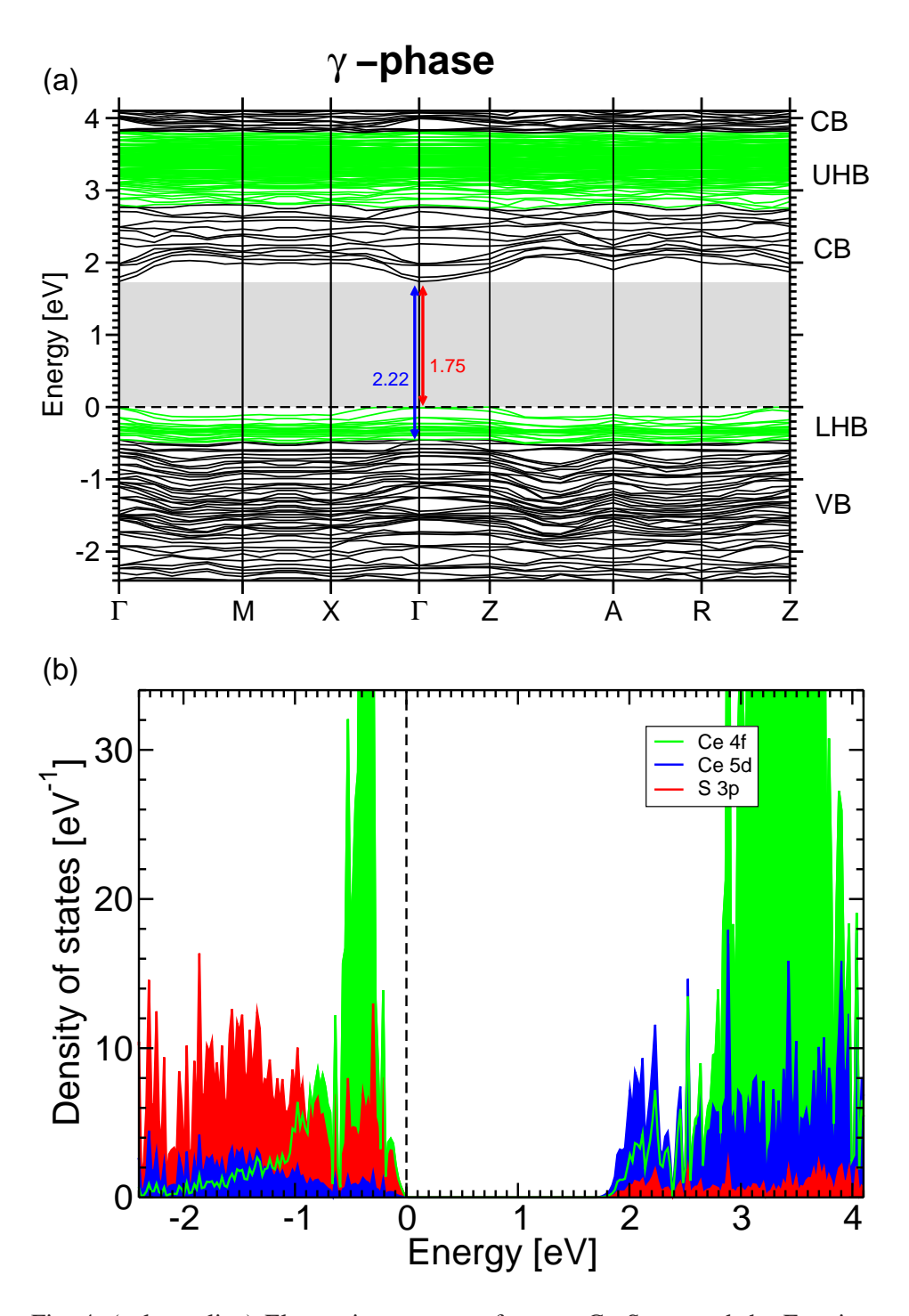


Fig. 4. (color online) Electronic structure of pure γ -Ce₂S₃ around the Fermi energy. (a) Band structure and (b) partial density of states calculated for the fully optimized system Ce₁₆S₂₄ (space group $I\bar{4}2d$). More details are given in the legend of Fig. 2.

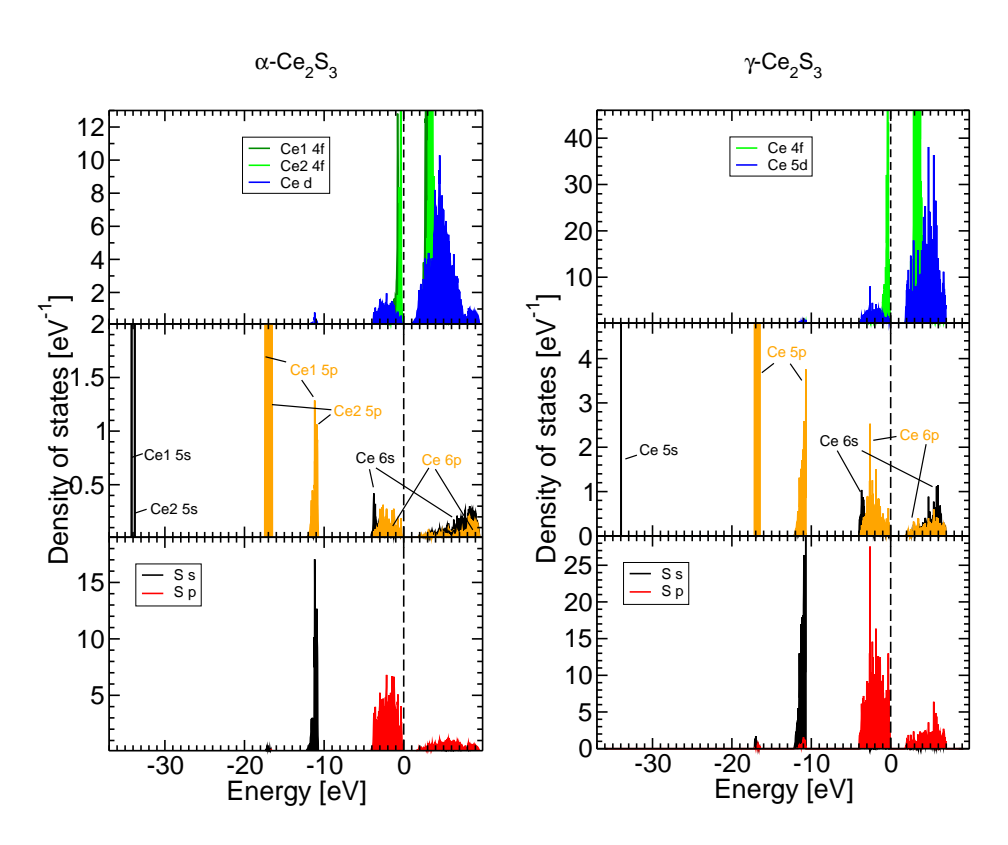


Fig. 5. (color online) Calculated partial density of states of two Ce_2S_3 modifications in the energy range between -37 and 10 eV.

List of Tables

1	Calculated lattice parameters and selected interionic distances, Ce1–X and Ce2–X, of α -Ce ₂ S ₃ compared with data obtained from	
	the x-ray diffraction measurements of Ref. [11]. The notation is according to that of Fig. 1(a). All distances are given in Å.	34
2	Comparison of calculated and measured lattice parameters and	

Comparison of calculated and measured lattice parameters and selected interionic distances of γ-Ce₂S₃. The calculated data have been obtained from the fully optimized supercell of Ce₁₆S₂₄ as depicted in Fig. 1(c). The experimental data has been taken from Ref. [34]. All values are given in Å.

Table 1 Calculated lattice parameters and selected interionic distances, Ce1–X and Ce2–X, of α -Ce₂S₃ compared with data obtained from the x-ray diffraction measurements of Ref. [11]. The notation is according to that of Fig. 1(a). All distances are given in Å.

Lattice (space	Interionic Distances									
			X	Ce1		Ce1		Co	Ce2	
Parameters	Exp.	Calc.		Exp.	Calc.	Exp.	Calc.			
а	7.532	7.565	S1			2.850	2.872			
b	4.097	4.119	S1'	3.100,	3.062,	3.040	3.056			
				3.135	3.161					
c	15.728	15.722	S2	2.983	2.998	2.883	2.893			
$\Delta V/V_{exp}$ [%]		0.95	S2'	4.727	4.761	2.976	2.988			
			S3	3.006	3.018	2.897	2.893			
			S3'	2.850	2.853	4.696	4.719			
			Ce1	4.031	4.029	4.015	4.035			
			Ce2	4.015	4.035	4.097	4.119			

Table 2 Comparison of calculated and measured lattice parameters and selected interionic distances of γ -Ce₂S₃. The calculated data have been obtained from the fully optimized supercell of Ce₁₆S₂₄ as depicted in Fig. 1(c). The experimental data has been taken from Ref. [34]. All values are given in Å.

Lattice (C	Quasi cub	pic)	Dista	ances	
Parameter	Exp.	Calc.		Exp.	Calc.
а	8.637	8.677	$r_{min}(\text{Ce}\cdots\text{Ce})$	4.040	3.958
c	8.637	8.641 ^{a)}	$\langle r(\text{Ce-S}) \rangle^{c)}$	2.896	2.898
$\Delta V/V_{exp} imes 100$		0.97	$\langle r(\text{Ce-S'}) \rangle^{c)}$	3.087	3.086
			$r(Q-S)^{b}$	2.896	2.988
			$r(Q-S')^{b)}$	3.087	3.208
			$r_{min}(\mathbf{Q}\cdots\mathbf{Q})^{b}$	7.785	7.779

a) c/3 of the tetragonal supercell of Fig. 1(c).

b) Q is the center of the voids on the cation sublattice.

c) The notation is according to Fig. 1(b).